NJC

PAPER

Cite this: *New J. Chem.*, 2015, 39, 9487

A new pyrazolyl dithioate function in the precursor for the shape controlled growth of CdS nanocrystals: optical and photocatalytic activities†

Gopinath Mondal,[a] Moumita Acharjya,[a] Ananyakumari Santra,[a] Pradip Bera,[a] Sumanta Jana,[b] Nimai Chand Pramanik,[c] Anup Mondal[b] and Pulakesh Bera*[a]

Received (in Montpellier, France) 26th August 2015,
Accepted 25th September 2015

DOI: 10.1039/c5nj02274f

www.rsc.org/njc

The dithiocarbazate functionalized 3,5-dimethyl pyrazole ligands and their cadmium(II) complexes *e.g.*, $[Cd(mdpa)_2Cl_2]$ (where mdpa is the methyl ester of 3,5-dimethyl pyrazole-1-dithioic acid) and $[Cd(bdpa)_2Cl_2]$ (where bdpa is the benzyl ester of 3,5-dimethyl pyrazole-1-dithioic acid) have been synthesized. The complexes are used as single-source precursors (SPs) for the synthesis of spherical and rod-like CdS nanocrystals in a solvothermal process without using any external surfactants. *In situ* generated thiols (CH_3SH in the case of the mdpa complex and $PhCH_2SH$ in the case of the bdpa complex) in thermolysis of the SP govern the growth of nanocrystals. The spherical and rod shaped CdS nanocrystals are produced in the presence of CH_3SH and $PhCH_2SH$, respectively. A possible growth mechanism of nanocrystals based on the preferential thiol bonding to the nucleus is discussed. The nanocrystals were characterized by X-ray diffraction (XRD), transmission electron microscopy (TEM), high resolution transmission electron microscopy (HRTEM) and X-ray photoelectron spectroscopy (XPS). The UV-Vis spectroscopic studies of CdS nanocrystals show the quantum confinement effect with a band gap of 2.2 eV to 2.6 eV, and the narrow intense PL emissions of the samples are red-shifted (λ_{max} = 570 nm) due to trap-related electron–hole recombination. The CdS nanocrystals are successfully applied in the photodegradation of rose bengal (RB) and methylene blue (MB) dyes under visible light.

1. Introduction

Nanostructured metal sulphides have been extensively studied due to their importance in interpreting the quantum size effect[1] and applications in a variety of devices such as solar cells,[2–4] light-emitting diodes,[5] sensors,[6,7] lithium-ion batteries[8] and fuel cells.[1,7] Additionally, many metal sulphide semiconductor materials have been used as sensitizers for photoinduced redox conversion of many organic pollutants, such as organic dyes, to form eco-friendly end products.[9,10] Metal sulphides are a major group of materials that provide the crystal chemists a high throughput due to their diverse dimensionality in structure.[11] In this context, CdS is one of the important n-type semiconducting materials belonging to groups II–VI showing different physical, chemical and optical properties with respect to the corresponding "bulk" material.[12]

Various chemical methods have been used to synthesize CdS nanocrystals including solid state reactions,[13] self-propagating high temperature synthesis,[14] pyrolysis of single-source metal–organic precursors,[15–21] solvothermal syntheses,[22,23] microwave techniques,[24] ultrasonic irradiation,[25] hot injection method,[26] and so on. In these processes, surfactants like trioctyl phosphine (TOP), trioctyl phosphine oxide (TOPO), cetyl trimethyl ammonium bromide (CTAB), hexadecyl amine (HDA), hexaphosphonic acid (HPA) *etc.* were used which are highly toxic and have a toxic effect on the environment. So it remains an intriguing and ongoing challenge to exploit reliable, reproducible, robust, eco-friendly and facile methods for the synthesis of high quality CdS nanocrystals. In that respect, a surfactant-less solvothermal route using single-source precursors is one of the best green synthetic methods employed for the preparation of CdS nanocrystals. Shape control and size tuning of the nanocrystals can be achieved by tailoring the reaction parameters like concentration of the SP, reaction time, temperature, solvent types and use of surfactants of different concentrations. But the single-source route is often embodied with demerits like broad size distribution and polydispersity of nanocrystals. However, few single-source

[a] *Post Graduate Department of Chemistry, Panskura Banamali College, Vidyasagar University, Midnapore (E), West Bengal-721152, India. E-mail: pbera.pbc.chem@gmail.com*
[b] *Department of Chemistry, Indian Institute of Engineering Science and Technology (IIEST), Shibpur, West Bengal-711103, India*
[c] *Aerogel Laboratory, Centre for Materials for Electronics Technology (C-MET), Athani, M G Kavu PO, Thrissur 680581, India*

† Electronic supplementary information (ESI) available. See DOI: 10.1039/c5nj02274f

precursors have been developed to produce nanocrystals of reasonable monodispersity which certainly provided the clear distinction of nucleation and growth processes. Recent studies have shown that the shape and size of nanocrystals highly depended on the rate of nucleation and monomer concentration at any instant along with other parameters like reaction time and temperature.[27] The solvent type used also has a great influence in deciding the particle morphology. Very recently, it was shown that the precursor itself acts as preformed nuclei capable of structural rearrangement enabling the separation of nucleation and growth processes.[28–30] Thus size tuning is possible only by modifying the organic chromophores of the ligand in SPs. However, the SP-directed shape controlled synthesis of nanocrystals is practically rare. Our present work uses two new pyrazolyl dithioate functionalized SPs in the shape controlled synthesis of CdS nanocrystals. Thermolysis of SPs furnished the products whose shape varies with the functional group present in the pyrazolyl dithiocarbazate precursor.

Dithiocarbamates (SS donor) and dithiocarbazates (NS donor) are a special class of compounds with a similar backbone[31] which can easily form metal complexes of low decomposition temperature. These low-melting complexes are exclusively used as single-source molecular precursors for the synthesis of MS nanoparticles.[17] Many dithiocarbamate–metal complexes have been successfully used earlier in the preparation of metal sulphide nanoparticles.[15–20] Other S-containing organic molecules such as thiosemicarbazide,[32] xanthates,[27] biurate[15,20] and thiourea[28] have also been used in the preparation of MS nanocrystals with different shapes, sizes and crystallinities. Very recently designing ligands for the synthesis of metal–organic precursors has been popularized for the facile synthesis of good quality nanocrystals. Revaprasadu *et al.* used heterocycle based dithiocarbamates *e.g.*, Cd(II)-piperidine dithiocarbamate and Cd(II)-tetrahydroisoquinoline dithiocarbamate as precursors for the synthesis of HDA and TOPO capped CdS nanorods, bipods and tripods.[20] *N*,*N*′-Dioctyl/dicyclohexyl/diisopropyl/tetraethylenethiourea and dithiourea cadmium complexes are used as single precursors for the solvothermal synthesis of CdS nanocrystals.[28] Our group used various main group metal complexes of dithiocarbazates to synthesize different metal sulphide nanocrystals.[33–38] To obtain anisotropic nanocrystals, a kind of structure directing agent is needed.[28] The structure directing agents are generally the surfactants or the solvents used in the thermolysis. Scholes *et al.* used the cadmium(II)-complexes of thiosemicarbazide and selenosemicarbazide that uniquely yield rod-shaped CdS and CdSe nanocrystals, respectively, without the aid of any external shape-directing agent.[28] The metal–organic single-source precursors themselves dictate the growth direction of the nanocrystals. We reported earlier the preparation of CdS nanocrystals (spheres and rods) thermolysing the Cd(II)-complex of S-benzyl dithiocarbazate in chelating solvents like hexamethylenediamine, ethylene glycol, ethylene diamine, and hydrazine hydrate.[34] Rod shaped CdS particles are obtained in a solvothermal process using the Cd–dithiocarbazate complex in hexamethylenediamine solvent.[33] It is assumed that the long chain diamine acts as a structure-directing agent for the anisotropic growth of nanocrystals. But still the mechanism of shape evolution is unclear. To obtain an insight into the influence of the structure of a SP on evolution of isotropic nanocrystals, we synthesized two functionalized pyrazolyl dithiocarbazates as building blocks of two new precursors *viz.* $[Cd(mdpa)_2Cl_2]$ and $[Cd(bdpa)_2Cl_2]$, and used them in shape controlled synthesis of nanocrystalline CdS spheres and rods, respectively, in a solvothermal process. CdS is one of the important n-type semiconducting materials belonging to groups II–VI and used as a catalyst for advanced photooxidation of organic pollutants owing to its appropriate band potential for redox reaction. The prepared CdS shows excellent photocatalytic activity in photodegradation of organic dyes (RB and MB) under visible light irradiation.

2. Experimental section

2.1 Chemicals

Cadmium chloride (Merck), carbon disulfide (Merck), acetyl acetone (Merck), methyl iodide (Spectrochem), benzyl chloride (Merck), ethylene diamine (Himedia), ethylene glycol (Himedia), and *N*,*N*-dimethyl sulphoxide (Merck) were all of analytical grade and used without further purification. Solvent ethanol (Changshu Yangyuan Chemical, China) was dried and distilled before use.

2.2 Synthesis of ligands mdpa and bdpa

2.2.1 Methyl-3,5-dimethyl pyrazole-1-carbodithioc acid (mdpa). The ligand, methyl ester of 3,5-dimethyl pyrazole-1-carbodithioic acid (mdpa), was prepared in a reaction of 3,5-dimethylpyrazole (0.97 g, 10.0 mmol) in tetrahydrofuran (15 mL) with carbon disulfide (0.99 g, 13 mmol) and methyl iodide (1 mmol, 2.12 g) in an ice bath temperature with constant stirring.[38] The stirring was continued for an additional 1 hour whereupon a yellow coloured compound of methyl ester of 3,5-dimethyl pyrazole-1-carbodithioc acid (mdpa) separated out, which was filtered off, washed with water and dried over silica gel. Yield: 82%. M.P. (decomposed): 30 °C. Anal. calc. for $C_7H_{10}N_2S_2$: C, 45.13; H, 5.41; N, 15.04; S, 34.42. Observed: C, 45.01; H, 5.72; N, 15.48; S, 33.88. IR (cm^{-1}): 3398–3476, ν(O–H); 863, ν(C═S); 1585, ν(C═N); 1490, ν(C–N).

2.2.2 Benzyl-3,5-dimethyl pyrazole-1-carbodithioc acid (bdpa). Benzyl-3,5-dimethylpyrazole-1-carbodithioic acid (bdpa) was prepared by the condensation of acetyl acetone (10 mmol, 1 mL) and S-benzyl dithiocarbazate (10 mmol, 1.9 g)[33,34] in 20 mL of dry ethanol followed by the addition of 5 mL of glacial acetic acid. The cooled light yellow product was filtered off and washed with dry ethanol. M. P. 86 °C. Anal. calc. for $C_{13}H_{14}N_2S_2$: C, 59.51; H, 5.38; N, 10.68; S, 24.44. Observed: C, 59.5; H, 5.40; N, 10.70; S, 24.50. IR (cm^{-1}): 3270, ν(O–H); 1572, ν(C═N); 1422, ν(C═C); 1020, ν(N═N);789, ν(C═S).

2.3 Synthesis of SP complexes $[Cd(mdpa)_2]Cl_2$ and $[Cd(bdpa)_2]Cl_2$

For the preparation of SPs, 2.00 g of $CdCl_2{\cdot}H_2O$ (10 mmol) dissolved in 20 mL of dry ethanol was added to the ligand solution (20 mmol in 20 mL dry ethanol) with constant stirring for 10 minutes. Then the resulting mixture was refluxed in water bath temperature for 2 hours whereupon a light yellow

precipitate was obtained. The precipitate was then filtered off, washed with ethanol and dried in vacuum over silica gel. For $[Cd(mdpa)_2Cl_2]$: yield 90%, MP (decomposition temperature) 145 °C, Λ_m = 15 Ω^{-1} cm^2 mol^{-1}, IR (cm^{-1}) 1571, ν(C═N); 789, ν(C═S) and for $[Cd(bdpa)_2Cl_2]$: yield 82%, MP (decomposition temperature) 178 °C, Λ_m = 18 Ω^{-1} cm^2 mol^{-1}, IR (cm^{-1}) 1586, ν(C═N); 774, ν(C═S).

2.4 Synthesis of CdS nanocrystals

0.50 mmol of precursor was taken with 15 mL of ethylenediamine in a 50 mL two-necked round bottom flask placed with a condenser and a thermocouple adaptor. The flask was degassed at room temperature for 5 minutes and then filled with inert nitrogen gas. The resulting solution was then gradually heated to 150 °C and the reaction temperature maintained for 30 minutes, immediately after which the reaction was stopped by adding cold ethanol.

The yellow suspension was collected through centrifugation and washed 4 to 5 times with cold and dry ethanol. The same set of experiments was also done in EN at 180 °C for 1 hour with the SP. The nanoparticle synthesis at 200 °C was done in DMSO. Dry powder of CdS nanocrystals was dried at 120 °C for 1 hour in a vacuum oven. The reaction parameters and the shape of the nanocrystals are given in Table 1.

2.5 Characterization

The elemental analysis (C, H, N, and S) of the complex was performed using a FISONS EA-1108 CHN analyzer. The FTIR spectra (4000 cm^{-1}–500 cm^{-1}) were recorded on a Perkin Elmer Spectrum Two spectrophotometer. The samples were prepared using KBr pellets technique. The molar conductance values of the complexes were measured in an ethanolic solution using a Systronics model 304 digital conductivitymeter. The thermogravimetry analysis of the precursor was carried out on a Perkin Elmer TGA 4000 instrument at a heating rate of 10 C min^{-1} under nitrogen. UV-Visible absorption spectra were recorded on a Perkin Elmer Lambda 35 spectrophotometer in the 200–800 nm wavelength range at room temperature and photoluminescence (PL) spectra were recorded on an F-7000 FL spectrophotometer. The photocatalytic activity was observed under a 250 W electric lamp. Powder X-ray diffraction (XRD) patterns of the NCs were recorded using a Seifert XDAL 3000 diffractometer using graphite-monochromated Cu-Kα radiation (λ = 1.5418 Å) with a scan rate of 5° min^{-1} over a range of $5^\circ < 2\theta < 80^\circ$ with steps of 0.02° and a scintillation detector operating at 40 kV and 40 mA. TEM and HRTEM characterization of cadmium sulfide nanocrystals was performed using a JEOL JEM-2100F EMI7220019 at an accelerating voltage 200 kV. The TEM samples were prepared by placing a drop of dilute ethanol dispersion of nanocrystals on the surface of a 200-mesh carbon-coated copper grid. EDX spectra were recorded on a JEOL JSM-5800 scanning microscope, OXFORD ISIS-300 microanalytical system. XPS was performed on an AXIS NOVA X-ray photoelectron spectroscope, using monochromatic Al-Kα radiation with an anode voltage of 15 kV and an emission current of 10 mA, the low resolution survey spectrum was recorded with a pass energy of 160 eV, the high resolution spectrum was recorded with a pass energy of 20 eV, and the quantification was performed by peak area measurement. Photocatalytic activity of CdS nanoparticles was studied with 50 mL of 2.1 × 10^{-5} M and 1.7 × 10^{-5} aqueous solutions of RB and MB, respectively, in a 100 mL beaker using a visible light source. A 250 W indoor fluorescent lamp was used as a light source. The concentration of the dye after photocatalytic degradation was determined using a Perkin Elmer Lambda 35 UV-Vis spectrophotometer.

3. Results and discussion

3.1 Synthesis and characterization of SPs

The condensation product of esters of dithioic acid *viz.* S-methyl dithiocarbazate (sdtc) and S-benzyl dithiocarbazate (bdtc) with acetyl acetone (acac) easily produces N^1 substituted 3,5-dimethyl pyrazole. In other words, the insertion of C(S)SR (carbodithioate) into the N–H bond of 3,5-dimethyl pyrazole gives the title ligands mdpa and bdpa. Pyrazole is considered to be the most flexible ligand in coordination chemistry due to its diatopic nature and the coordination flexibility of the pyrazolido (pz-) ion.[39] The ease of synthesis of pyrazolyl ligands and their varieties of coordination modes with fascinating chemistry are the reasons for the study. The rich chemistry of pyrazole and its derivatives is attributed to several chemical merits such as the presence of a localized lone pair of electrons on an in-plane orbital and the presence of low energy anti-bonding vacant π* orbitals of the aromatic system guaranteed their π-acidity.[39] Keeping all this in mind, we choose the functionalized pyrazolyl ligands for the synthesis of functionalized SPs so that they can provide special properties during nanocrystal growth.

Solid state isolation and satisfactory results of the elemental analysis, conductance values and spectral studies reveal that the ligands and their cadmium complexes are of good purity and they are significantly stable in air. The ligands and their Cd(II)-complexes were characterized by means of elemental

Table 1 Reaction conditions and analytical results

$[Cd(mdpa)_2]Cl_2$					$[Cd(bdpa)_2]Cl_2$				
Solvent (mL)	Temperature (°C)	Time (min)	Shape	Size (nm)	Solvent (mL)	Temperature (°C)	Time (min)	Shape	Size (nm)
EN (15)	150	30	Spherical	8	EN (15)	150	30	Rod shape	$80^a/10^b$
EG (15)	180	60	Spherical	10	EG (15)	180	60	Rod shape	$136^a/10^b$
DMSO (15)	200	90	Spherical	12	DMSO (15)	200	90	Rod shape	$140^a/10^b$

[a] Average length. [b] Average diameter.

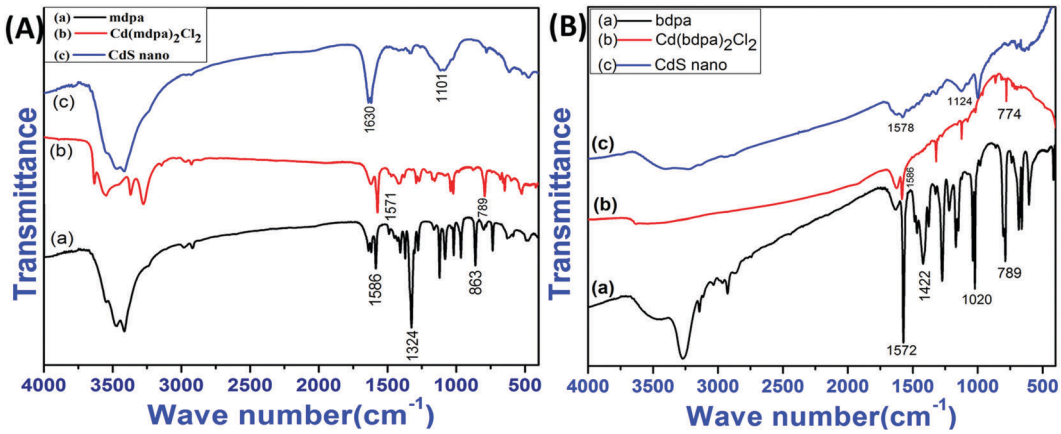

Fig. 1 FTIR spectra: (A) [mdpa, $Cd(mdpa)_2Cl_2$ and CdS nanocrystals derived from $Cd(mdpa)_2Cl_2$] and (B) [bdpa, $Cd(bdpa)_2Cl_2$ and CdS nanocrystals derived from $Cd(bdpa)_2Cl_2$] in EG at 180 °C.

analyses, conductivity measurements, FTIR and mass spectroscopy. The molar conductivity values of $\sim 10^{-3}$ M solution in methanol prove the non-ionic nature of the cadmium complexes. The most probable composition of the cadmium complexes of mdpa and dbpa is $[Cd(mdpa)_2Cl_2]$ and $[Cd(bdpa)_2Cl_2]$, respectively, based on the conductance and FTIR results. The similar coordination behavior is also observed in the cadmium complex of dithiocarbamate.[40] FTIR spectra of the free ligands, cadmium complexes and the derived CdS nanoparticles from the Cd-complex precursor are shown in Fig. 1. The very broad bands typical for water in the range of 3250–3470 cm^{-1} region in the IR spectra are the proof of the hygroscopic nature of mdpa, bdpa and $[Cd(mdpa)_2Cl_2]$. A careful comparison of FTIR spectral data on the complexes with those of the ligands furnished considerable information regarding the mode of bonding of ligands. The peaks in the spectrum of complexes are less in number and quite sharp than the ligand's spectrum clearing proving the strong bonding of ligands with cadmium. A further redundancy of peaks in the spectrum of CdS nanoparticles (curve c in Fig. 1A and B) clearly indicates the non-adherence of ligands to the surface of nanoparticles. The weak peaks appearing at 1630 cm^{-1} for CdS derived from $[Cd(mdpa)_2Cl_2]$ (curve c in Fig. 1A) or at 1528 cm^{-1} for CdS derived from $[Cd(bdpa)_2Cl_2]$ (curve c in Fig. 1B) may be due to the presence of trace amounts of nitrogenous organic fragments in the samples. The presence of a strong band at 1585 cm^{-1} for mdpa or at 1572 cm^{-1} for bdpa due to $\nu_{C=N}$ (pyrazole ring) shifted to the higher frequency by 12–25 cm^{-1} in their respective complexes. These data indicate that the tertiary nitrogen atom of the pyrazole ring was involved in bonding to Cd(II). The coordination of the thione sulphur atom to cadmium is indicated by a decrease of the $\nu_{C=S}$ band from 860 cm^{-1} in mdpa or 861 cm^{-1} in bdpa to 792 cm^{-1} in $[Cd(mdpa)_2]Cl_2$ or 784 cm^{-1} in $[Cd(bdpa)_2Cl_2]$, respectively. The positive shifts of the ν_{N-Npz} frequencies at 1292 cm^{-1} for mdpa or at 1250 cm^{-1} in bdpa to *ca.* 30 cm^{-1} on complexation with Cd(II) indicated the involvement of pyrazolyl tertiary nitrogen in bonding. Similar results are also found for the cadmium complexes of ligands with a similar structural backbone.[40]

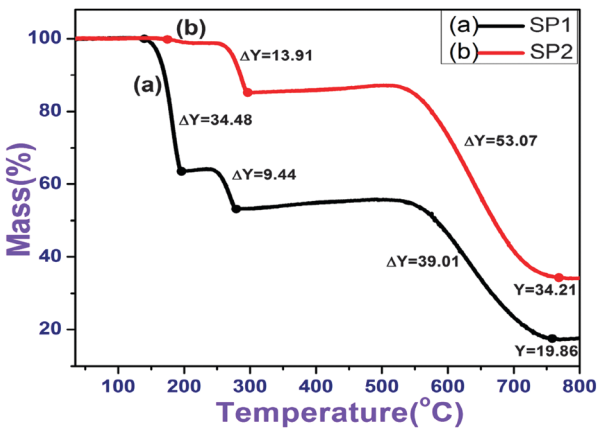

Fig. 2 TG analysis of (a) $[Cd(mdpa)_2Cl_2]$ (SP1) and (b) $[Cd(bdpa)_2Cl_2]$ (SP2).

Thermogravimetry analysis is conducted to study the thermal behavior and suitability of the precursors for the preparation of CdS. The TGA curves of $[Cd(mdpa)_2Cl_2]$ and $[Cd(bdpa)_2Cl_2]$ are given in Fig. 2. The three-step decomposition process of the precursor $[Cd(mdpa)_2Cl_2]$ starts at the temperature of 120 °C and is completed by 750 °C. The first step decomposition (found mass loss 34.48%) is accompanied by the combined loss of one Cl and one ligand unit except for one sulfur atom (*ca.* 34.08%) (see ESI†). The second step of mass loss is attributed to the loss of a SCH_3 unit (*ca.* 9.44%) giving a residue which is stable up to 550 °C. In the final step of decomposition (39.01%), the residual ligand unit is lost to form CdS which again loses the surface trapped S at higher temperature to finally form the metallic Cd residue (*ca.* 20.21%). The decomposition of $[Cd(bdpa)_2Cl_2]$ started at 120 °C following two major decomposition steps. The first step is attributed to the loss of the $-CH_2Ph$ unit (*ca.* 12.85%) giving a residue that is stable up to *ca.* 550 °C. The major loss occurred in the last step of decomposition which is attributed to the loss of all organic materials followed by the reversible addition of gaseous sulfur atoms to the metallic cadmium giving a residue $[CdS]S_3$ (*ca.* 33.89%). The TGA curves of the precursors also serve as a guideline for deciding the thermolysis temperature of the precursors. The thermolyses of

the SPs were performed at 150 °C, 180 °C and 200 °C to avoid any incomplete decomposition.

3.2 Morphology and characterization of CdS NPs

X-ray diffraction (XRD) patterns for the nanocrystals synthesized at different temperatures are shown in Fig. 3. The diffraction patterns of the samples are indexed to the wurtize (hexagonal) phase of CdS with characteristic (100), (002), (101), (102), (110), (103), and (112) peaks (JCPDS number 041-1049). The broad peak in the XRD patterns (Fig. 3c) of the sample obtained from EG at a lower growth temperature (150 °C) reveals the small size and amorphous nature of the sample whereas sharp peaks (Fig. 3a and b) are observed for the samples at higher growth temperatures.

The morphology and microstructures of the as-synthesized CdS nanocrystals were characterized by TEM and SEM analyses. Fig. 4 shows TEM and high resolution TEM pictures of CdS nanocrystals prepared under different reaction conditions and the average particle sizes as calculated from TEM images are given in Table 1. Nearly spherical CdS particles can be seen in the high resolution TEM images (Fig. 4A and B) of the samples prepared from $[Cd(mdpa)_2Cl_2]$ using EG and EN, respectively, at 150 °C. The sizes of synthesised nanocrystals are found to be 8–10 nm under various reaction conditions. At higher reaction temperatures *e.g.*, 180 °C the product morphology is the same but a very small increase of the size is observed. The SAED image of single spherical CdS nanocrystals prepared from $[Cd(mdpa)_2Cl_2]$ is indicative of clear crystallinity of the particles with all possible diffractions of planes as shown in Fig. 4C. The measured lattice spacing for the CdS nanocrystals from EG at 180 °C is found to be 3.3 nm (inset of Fig. 4B) which corresponds to the diffraction of the (002) plane. It has been observed that the SP functionalized with a $-SCH_3$ group *i.e.*, $[Cd(mdpa)_2Cl_2]$ results in only spherical morphology irrespective of the solvent used in the thermolysis. The high resolution TEM images of the samples obtained from $-SCH_2Ph$ functionalized SP *i.e.*, $[Cd(bdpa)_2Cl_2]$ in EG and EN at 180 °C are given in Fig. 4D and E, respectively. An urchin-like CdS hierarchical nanostructure resulted irrespective of the solvent used in the thermolysis of $[Cd(bdpa)_2Cl_2]$. The nanostructure is composed of many nanorods which self-assembled into an urchin-like architecture. The average diameter of the nanorods is higher in the centre of the structure than the open ended side by about 4 to 5 times indicating the non-uniform nature of the nanoarchitectures. These kinds of coarse architectures are capable of showing catalytic activity. The *d*-spacing observed (Fig. 4F) corresponds to the (002) plane of hexagonal CdS. The growth direction of these (002) facets is anisotropic, suggesting the retardation of a large number of (110) facets in the nanostructures. In addition to determining the appropriate crystallinity the energy-dispersive X-ray spectroscopy (EDX) analysis of CdS nanocrystals was done in a carbon coated copper grid, which confirmed the elemental composition of Cd : S ≈ 1 : 1, and no precursor element remained after the reaction (Fig. S1 and S2, ESI†).

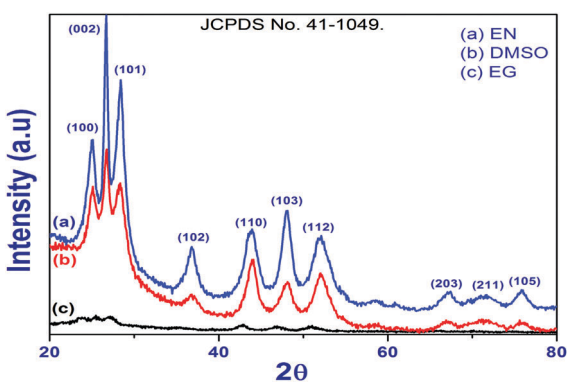

Fig. 3 X-ray diffraction patterns of CdS nanocrystals prepared from $[Cd(bdpa)_2Cl_2]$ in EN (a), in DMSO (b) and $[Cd(mdpa)_2Cl_2]$ in EG (c) at 180 °C.

The XPS spectrum of the sample prepared from EN at 180 °C was recorded to check the atomic composition and surface chemistry. The Cd 3d spectrum has a doublet feature due to the spin orbit splitting resulting in $3d_{5/2}$ and $3d_{3/2}$ peaks with a spin orbit separation of 7.0 eV. The doublet peaks that were assignable to Cd $3d_{5/2}$ and Cd $3d_{3/2}$, respectively, were observed at 405.1 eV and 412.1 eV (Fig. 5) in the CdS sample. Apart from cadmium 3d, other core levels of interest in the materials are S 2p and S 2s. The S 2p spectrum exhibits a doublet arising from the spin orbit splitting in the 168.0 eV region that can be assigned to the form Cd–S– and the additional shake up peak at 166 eV is attributed to the oxidized sulfur species. The S 2s spectrum has a single peak feature appearing at a binding energy of 225 eV with shake up features which are observed earlier.[41] The oxygen on the surface at 532 eV may be due to the presence of chemisorbed oxygen.

3.3 Optical properties of CdS nanoparticles

Fig. 6 illustrates the UV-Vis absorption spectra of CdS nanocrystals dispersed in distilled ethanol at room temperature. A strong absorbance peak appeared at 480 nm (Fig. 6a) for the sample obtained from $[Cd(mdpa)_2Cl_2]$ in EG (180 °C) whereas the same characteristic bands are observed for the sample obtained from $[Cd(bdpa)_2Cl_2]$ at 480 nm and 485 nm (Fig. 6b and c) in EN (180 °C) and DMSO (200 °C). The band gap plots of $(\alpha h\nu)^2$ *vs.* $E(=h\nu)$ show the band gaps between the conduction and valence bands appearing at 2.2 eV, 2.5 eV and 2.6 eV (inset of Fig. 6) which indicates that they are good solar energy absorbers. Fig. 7 shows the PL emission spectra recorded at room temperature for the CdS nanocrystals obtained from different single source precursors. The spectra exhibit a narrow peak at 480 nm corresponding to the band-edge emission along with another red-shifted narrow intense peak in the 570 nm region. This red-shifted emission results from the trap related electron–hole recombination. It is to be noted that the samples obtained from different precursors emit at the same λ_{max} position with different emission intensities and peak widths. CdS obtained from $[Cd(bdpa)_2Cl_2]$ shows a narrow and sharp emission peak with higher intensity (Fig. 7b) than the CdS obtained from $[Cd(mdpa)_2Cl_2]$ (Fig. 7a) which proves the better electronic passivation of the CdS surface by $PhCH_2SH$ than CH_3SH. An emission peak in the 500–700 nm region is often

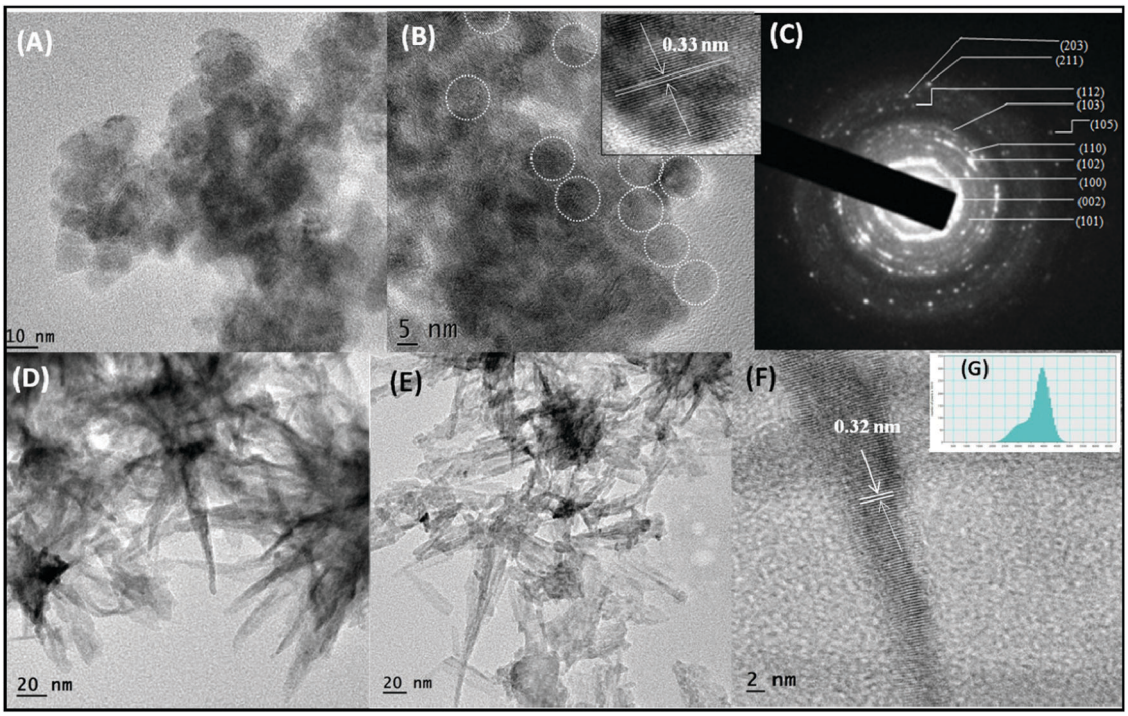

Fig. 4 TEM/HRTEM images of CdS nanocrystals obtained from $[Cd(mdpa)_2Cl_2]$ in EG at 150 °C (A), in EN at 180 °C (B) (inset showing the 'd' spacing value), and the SAED image of CdS nanocrystals from $[Cd(mdpa)_2Cl_2]$ in EG at 150 °C (C), TEM/HRTEM images of CdS nanocrystals obtained from $[Cd(bdpa)_2Cl_2]$ in EG at 180 °C (D), in EN at 180 °C (E and F), and a histogram of the sample (G).

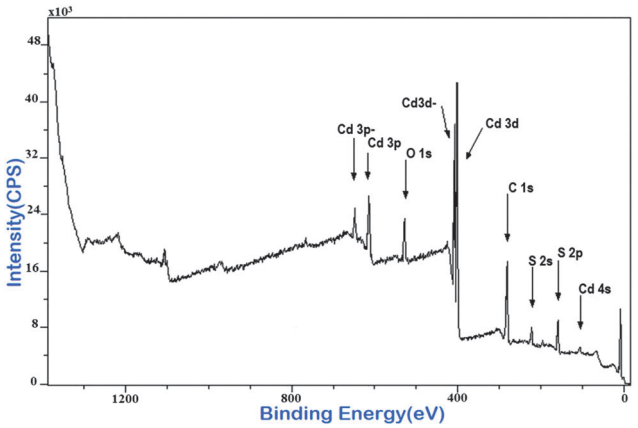

Fig. 5 XPS spectrum of CdS nanocrystals prepared from $[Cd(mdpa)_2Cl_2]$ using EG at 180 °C.

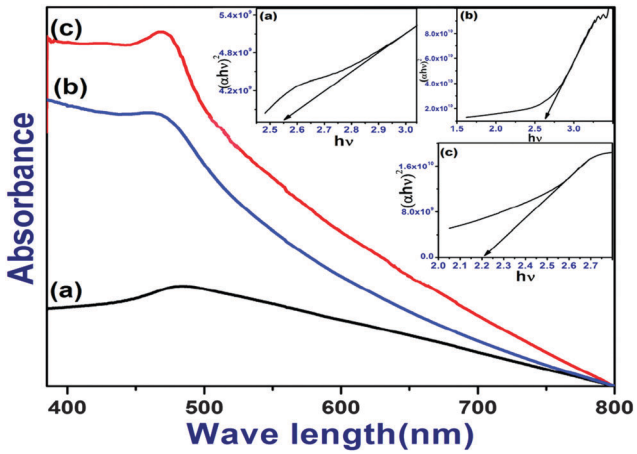

Fig. 6 UV-Vis spectra and band gap values of CdS nanocrystals obtained from $[Cd(mdpa)_2Cl_2]$ using EG at 180 °C (a), from $[Cd(bdpa)_2Cl_2]$ using EN (180 °C) (b), and from $[Cd(bdpa)_2Cl_2]$ using DMSO (200 °C) (c).

observed for CdS nanocrystals which is attributed to the recombination of trapped electrons–holes in the surface defect states.[42,43] The trap state emission is related to the surface chemistry and structure of the CdS nanocrystals. The band edge and trap-state photoluminescence indicate that the CdS sample has a suitable band gap position for photocatalytic decomposition of organic dyes under visible light irradiation.

3.4 Growth mechanism of CdS nanocrystals

In the SP method, factors that generally resulted in thermodynamic stable spherical products are the fast nucleation and the quick passivation of the seeded crystals in the presence of high concentration of stabilizing agent(s) at high reaction temperatures. Most of the SPs used so far in solvothermal methods produced spherical particles. On the other hand, the anisotropic growth of nanocrystals depends on several factors like the use of molecular template(s) and copious capping agents, and the lower activation energy of the SP.[15–20] In the case of dithiocarbamate and xanthate precursors, the M–S bond template is useful for controlling the shape of nanocrystals. Strouse *et al.* proposed that the metal clusters act as preformed

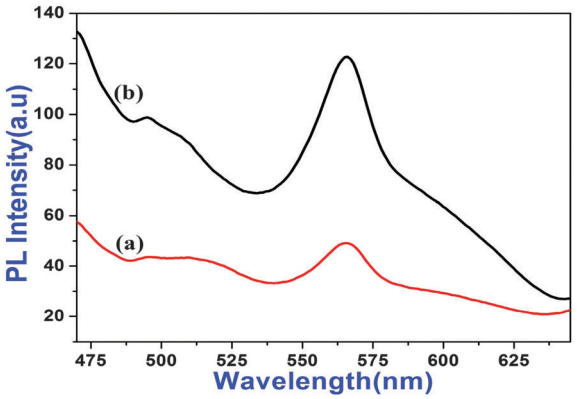

Fig. 7 PL emission spectra of CdS nanocrystals obtained from $[Cd(mdpa)_2Cl_2]$ using EN at 150 °C (a) and from $[Cd(bdpa)_2Cl_2]$ using DMSO at 200 °C (b).

nuclei which on structural rearrangement without dissolution enables the formation of 1D nanostructures.[30] Vittal *et al.* reported the shape controlled synthesis of Ag_2S nanoparticles using a 'nucleation initiator' *e.g.*, hexadecyl amine (HDA) which helps to separate nucleation and growth processes. It was proposed that the coordinating solvent plays a crucial role in deciding the particle morphology. CdSe nanorod formation is attributed to the higher coordinating nature of hexaphosphonic acid. Revaprasadu *et al.* reported the influence of solvent in controlled synthesis of CdS particles from the heterocyclic dithiocarbamate cadmium complex. Whereas spherical and elongated CdS nanoparticles were obtained from trioctyl phosphine oxide (TOPO) and hexadecyl amine (HDA) using the same heterocyclic precursor.

The effect of solvents is also reflected in our earlier reports on synthesis of spherical and rod-like particles from the same single-precursors *i.e.*, the cadmium complex of S-benzyl dithiocarbazate (sbdtc)[33,34] and/or the copper complex of S-methyl dithiocarbazate (smdtc)[36,38] formed by changing the solvent. We observed that the use of hexamethylene diamine (HMDA) and ethylene diamine (EN) solvents in the pyrolysis of $[Cd(sbdtc)_2Cl_2]_2$ selectively produces rod shaped 1D-CdS nanocrystals. Whereas other bidentate ligands like ethylene glycol (EG) and hydrazine hydrate (HH) produced only spherical products upon the thermolysis of $[Cd(sbdtc)_2Cl_2]_2$.[34] In particular, chelating diamines *e.g.*, EN or HMDA wherein two nitrogen atoms are separated by more than two carbon centres could form stable intermediate chelate complexes with the metal ion displacing ancillary ligands and thereby we proposed that the intermediate stable complex with coordinating solvent acts as a molecular template for the synthesis of anisotropic structure. Solvents other than chelating diamine could not be able to form intermediate stable complexes, as a consequence, thermodynamically stable spherical nanocrystals are expected. It was also observed that when the coordination environment of SPs is fairly stable with high level of coordination saturation, the primary SP structure was not affected by any kind of chelating/coordinating solvent.[37] The octa-coordinated Pb-complex of sbdtc always furnished spherical nanoparticles irrespective of the solvent used and the *in situ* generated organic fragment *e.g.*, CH_3SH stabilized the seeded crystals. Besides the solvent effect in crystal evolution, the special structural characteristics of SPs are responsible for anisotropic growth as reflected in the recent studies.[28,29] G. D. Scholes *et al.* proposed that Cd-complexes of thiosemicarbazide or seleno semicarbazide precursors with very low activation energy barrier (2.1 kJ mol^{-1}) were capable to produce rod-shaped CdS wherein the little higher activation energy in the range 18.0 kJ mol^{-1} furnished spherical CdS.[28]

In the present work, the extra stability to the SP was confirmed by incorporating the heterocyclic pyrazole with a thiolato environment. The smdtc and sbdtc were converted to mdpa and bdpa, respectively, which provide a stable environment to the cadmium centre so that the solvent participating in thermolysis cannot displace them. In our method, the solvent used to serve as the heat transferring medium. With heat the molecular transformation takes place in the coordination environment of $[Cd(mdpa)_2Cl_2]$ or $[Cd(bdpa)_2Cl_2]$. The internal rearrangement of the metal centre which can be regarded as a molecular template starts the nucleation and the growth of nanoparticles monitored by the fragmented thiol. Under the reaction conditions, $[Cd(mdpa)_2Cl_2]$ provides a small thiol ligand, CH_3SH, and $[Cd(bdpa)_2Cl_2]$ provides a relatively bulkier thiol, $PhCH_2SH$. The small thiol CH_3SH can bind strongly to all the facets of seed crystals giving only spherical nanoparticles where the bulkier thiol $PhCH_2SH$ preferentially binds the polar facets of nucleus giving an opportunity to grow the nanocrystals anisotropically. The proposed mechanistic pathways are summarized in Scheme 1. It is to be noted that the shape and size of the nanocrystals do not vary significantly with the concentration of the SP when other parameters were unaltered.

3.5 Photocatalytic activity of CdS NCs

The coarse architecture and the trap states in the crystal surface of CdS samples as ascertained from TEM and PL spectra, respectively, might be the reasons for them being good photocatalysts. Photon energy greater than the band gap energy of CdS produced electron–hole pairs. Such photogenerated electrons (e^-) and holes (h^+) are subsequently transferred to the surface of the crystal. Subsequently, e^- and h^+ react with H_2O and molecular O_2 to generate $OH^\bullet$ and O^{2-} radicals. These radicals decompose the organic dyes following free radical oxidation and reduction processes. To investigate the potentiality of the synthesised CdS nanocrystals as photo-catalysts, the catalytic performances were examined by photodegradation of RB and MB under visible light illumination. We have chosen RB and MB like organic dyes to test the photocatalytic activity, since these are fluorescent dyes and commonly used in textile, photographic and photochemical industries. The synthesised semiconducting CdS nanocrystals have been used as catalysts for photodegradation under visible light. Fig. 8 shows the time dependent UV-Vis spectral changes of RB and MB solutions in the presence of CdS nanocrystals under irradiation of light for 90 min and 65 min, respectively. Photocatalytic activity of CdS nanocrystals was studied with 50 mL aqueous solution of each 2.1×10^{-5} M RB and 1.7×10^{-5} M MB taken in a 100 mL beaker with 15 mg of CdS

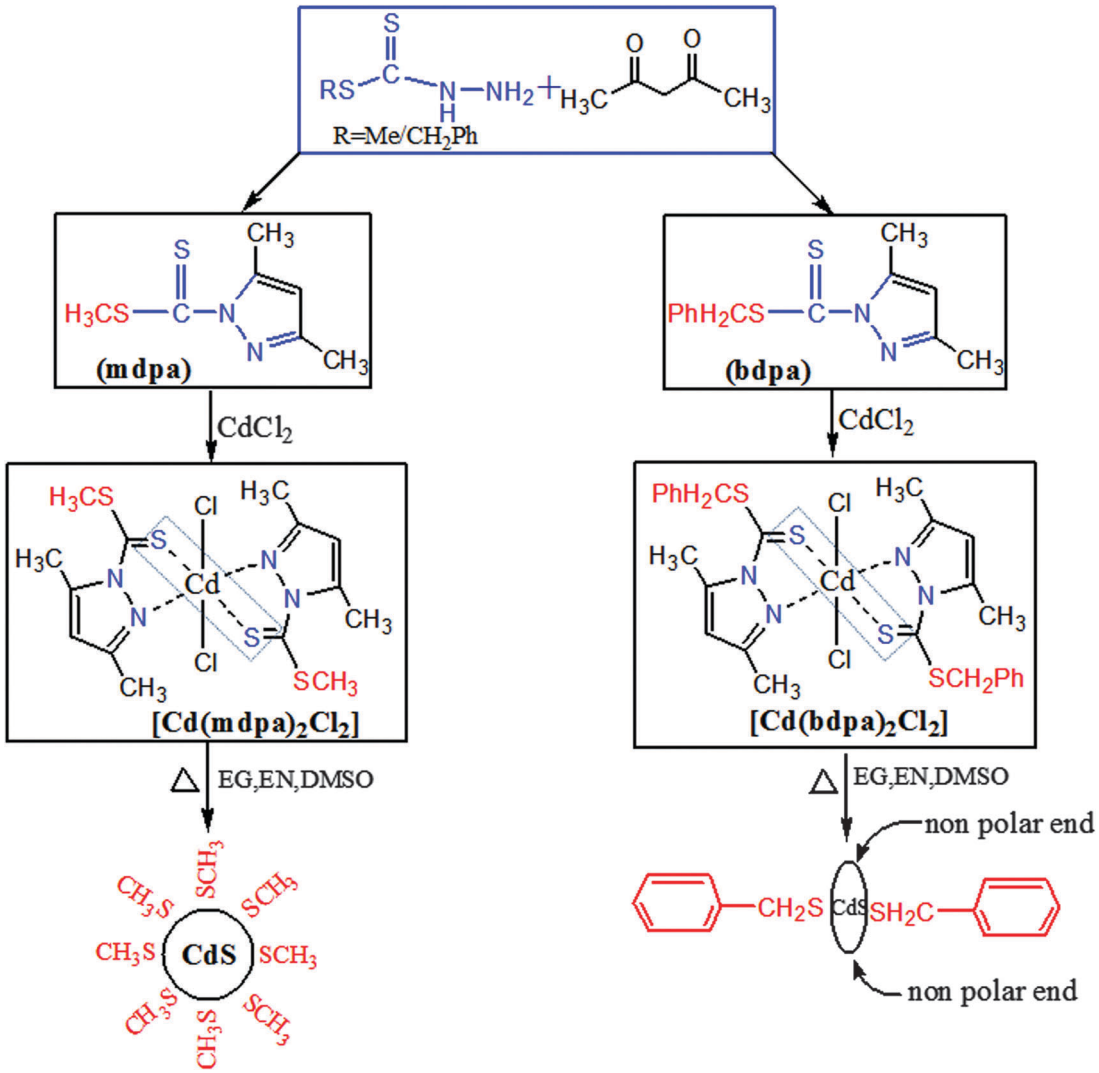

Scheme 1 Synthesis of SPs and the formation mechanism of CdS nanoparticles.

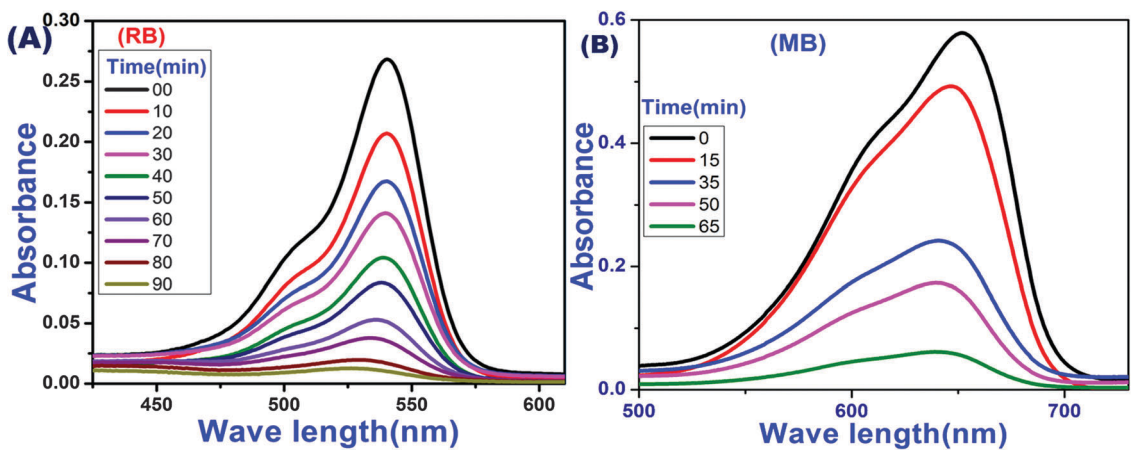

Fig. 8 Time dependent spectral changes of aqueous RB (A) and MB (B) solutions by CdS nanocrystals prepared from $[Cd(mdpa)_2Cl_2]$ and $[Cd(bdpa)_2Cl_2]$, respectively.

under a 250 W indoor fluorescent lamp used as a visible light source. The solutions were stored in dark to attain adsorption–desorption equilibrium for 40 min and then the solutions were exposed to visible light with magnetic stirring.

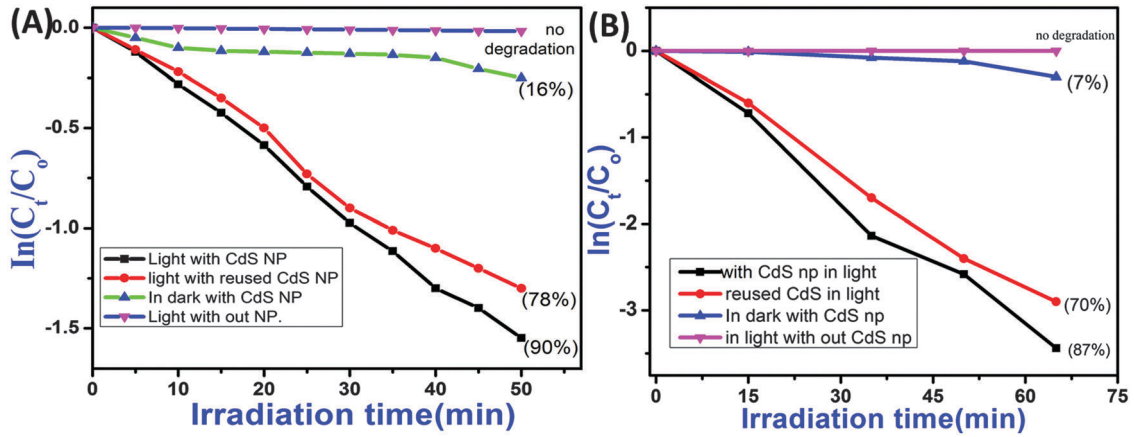

Fig. 9 Logarithmic change in the concentration of dyes as a function of irradiation time for (A) RB and (B) MB.

At a certain time interval 3 mL of solution was centrifuged and its absorption was measured on a UV-Vis spectrophotometer. The characteristic absorption peaks appeared at 540 nm and 650 nm for RB and MB solutions, respectively, and gradually decreased with irradiation time. After 90 min (for RB) and 65 min (for MB) of reaction time no new absorption peaks appeared, but the characteristic absorption bands of the dyes disappeared suggesting the complete photodegradation of RB and MB. In order to determine the kinetics of photodegradation, we plot $\ln(C_t/C_0)$ with irradiation time (t) (Fig. 9) in the equation $\ln(C_0/C_t) = kt$, where C_0 is the initial concentration of aqueous solution, C_t is the concentration at time t and k is the rate constant of the reaction. The measured k values are 3.5×10^{-3} min^{-1} and 4.8×10^{-3} min^{-1} for photodegradation in RB and MB, respectively. Degradation processes follow the first order kinetics.

4. Conclusion

Functionalization with alkyl and aryl carbodithioate groups in the N^1 position of 3,5-dimethyl pyrazole enables the chelation with soft sulphur and soft nitrogen donor atoms and forms easily air-stable cadmium(II) complexes *e.g.*, $[Cd(mdpa)_2Cl_2]$ and $[Cd(bdpa)_2Cl_2]$. TGA analyses of the complexes reveal their low decomposition temperature and suitability to act as single-source precursors for CdS nanocrystals. The single-source precursors are used in the shape controlled synthesis of hexagonal CdS nanocrystals in solvothermal processes without using external surfactants. The SP, $[Cd(mdpa)_2Cl_2]$, with the SCH_3 group in the structure always produced spherical CdS nanoparticles wherein the SP, $[Cd(bdpa)_2Cl_2]$, with the SCH_2Ph group selectively furnished rod-like CdS nanoparticles in the solvothermal reaction irrespective of the solvent used. We conclude that the evolution of spherical or rod shaped nanocrystals depends on the substituent(s) present in the precursor irrespective of the solvent used in the thermolysis. Different reaction temperatures and the nature of solvent have no profound effects on the shape other than the increase of the particle sizes. It is proposed that methane thiol (CH_3SH) in the case of $[Cd(mdpa)_2Cl_2]$ or benzyl thiol ($PhCH_2SH$) in the case of $[Cd(bdpa)_2Cl_2]$ was produced under the reaction conditions and acted as a structure directing agent as well as a stabilizing agent. Being a smaller thiol, CH_3SH can effectively bind all the facets of seeded crystals facilitating isotropic growth whereas bulky $PhCH_2SH$ binds selective polar facets forming rod shaped structures. The average sizes of the spherical nanocrystals are found to be 8 to 12 nm as evidenced by TEM analysis. The nanocrystals show a quantum confinement effect with a band gap of $\sim$2.2 eV. The PL emissions of the samples are red-shifted and are trap-related. The CdS nanocrystals have shown to be excellent catalysts in photodegradation of aqueous solution of rose bengal and methylene blue under visible light irradiation. We can predict that only a heating effect can cause solid state transformation of single molecular precursors to control the shape of nanocrystals. Further exploration is needed for better understanding of the structure–activity relationship of precursors and nanoproducts with respect to shape, size and crystallinity.

Acknowledgements

We gratefully acknowledge CSIR, Government of India [grant no. 1(2534)/11/EMR-II] and UGC, Government of India [F 42-280/2013(SR)] for financial support. The authors thank Professor Sang Il Seok, Department of Energy Science, Sungkyunkwan University, Suwon 440-746, South Korea for XPS analysis. We are thankful to Professor Dipankar Chattopadhyay of Centre for Research in Nanoscience & Nanotechnology (CRNN), University of Calcutta, JD-2, Salt Lake City, Kolkata 700098, West Bengal, India for TEM analyses.

References

1 M. R. Gao, Y. F. Xu, J. Jiang and S. H. Yu, *Chem. Soc. Rev.*, 2013, **42**, 2986–3017.
2 F. Cao, H. Wang, Z. Xia, X. Dai, S. Cong, C. Dong, B. Sun, Y. Lou, Y. Sun, J. Zhao and G. Zou, *Mater. Chem. Phys.*, 2015, **149–150**, 124–128.

3 K. Yuan, L. Chen, L. Tan and Y. Chen, *Chem. – Eur. J.*, 2014, **20**, 6010–6018, DOI: 10.1002/chem.v20.20.
4 J. Albero, J. N. Clifford and E. Palomares, *Coord. Chem. Rev.*, 2014, **263–264**, 53–64.
5 Y. L. Kong, I. A. Tamargo, H. Kim, B. N. Johnson, M. K. Gupta, T.-W. Koh, H-A. Chin, D. A. Steingart, B. P. Rand and M. C. McAlpine, *Nano Lett.*, 2014, **14**(12), 7017–7023.
6 J. Liu and D. Xue, *J. Mater. Chem.*, 2011, **21**, 223–228.
7 C. H. Lai, M. Y. Lu and L. J. Chen, *J. Mater. Chem.*, 2012, **22**, 19–30.
8 K. Chang and W. Chen, *Chem. Commun.*, 2011, **47**, 4252–4254.
9 W. T. Yao, S. H. Yu, S. J. Liu, J. P. Chen, X. M. Liu and F. Q. Li, *J. Phys. Chem. B*, 2006, **110**(24), 11704–11710.
10 A. K. Sahoo and S. K. Srivastava, *J. Nanopart. Res.*, 2013, **15**, 1591–1606.
11 S. Shen and Q. Wang, *Chem. Mater.*, 2013, **25**(8), 1166–1178.
12 D. Fan, M. Afzaal, M. A. Mallik, C. Q. Nguyen, P. O'Brien and P. J. Thomas, *Coord. Chem. Rev.*, 2007, **251**(13–14), 1878–1888.
13 W. Wang, Z. Liu, C. Zheng, C. Xu, Y. Liu and G. Wang, *Mater. Lett.*, 2003, 2755–2760.
14 A. Makino, *Prog. Energy Combust. Sci.*, 2001, **27**, 1–74.
15 K. Ramasamy, M. A. Malik, M. Helliwell, J. Raftery and P. O'Brien, *Chem. Mater.*, 2011, **23**(6), 1471–1481.
16 M. A. Malik, N. Revaprasadu and P. O'Brien, *Chem. Mater.*, 2001, **13**(3), 913–920.
17 M. A. Malik, M. Afzaal and P. O'Brien, *Chem. Rev.*, 2010, **110**(7), 4417–4446.
18 L. D. Nyamen, N. Revaprasadu, R. V. S. R. Pullabhotla, A. A. Nejo, P. T. Ndifon, M. A. Malik and P. O'Brien, *Polyhedron*, 2013, **56**, 62–70.
19 N. Srinivasan, S. Thirumaran and S. Ciattini, *J. Mol. Struct.*, 2012, **1026**, 102–107.
20 L. D. Nyamen, V. S. R. Pullabhotla, A. A. Nejo, P. Ndifon and N. Revaprasadu, *New J. Chem.*, 2011, **35**, 1133–1139.
21 A. L. Abdelhady, M. A. Malik and P. O'Brien, *J. Inorg. Organomet. Polym.*, 2014, **24**, 226–240.
22 D. Xu, Z. Liu, J. Liang and Y. Qian, *J. Phys. Chem. B*, 2005, **109**(30), 14344–14349.
23 J. Park, J. Joo, S. G. Kwon, Y. Jang and T. Hyeon, *Angew. Chem., Int. Ed.*, 2007, **46**, 4630–4660.
24 Y. Wada, H. Kuramoto, J. Anand, T. Kitamura, T. Sakata, H. Mori and S. Yanagida, *J. Mater. Chem.*, 2001, **11**, 1936–1940.
25 N. Ghows and M. H. Entezari, *Ultrason. Sonochem.*, 2011, **18**, 269–275.
26 C. B. Murray, C. J. Norris and M. G. Bawendi, *J. Am. Chem. Soc.*, 1993, **115**, 8706–8715.
27 N. Pradhan, B. Katz and S. Efrima, *J. Phys. Chem. B*, 2003, **107**(50), 13843–13854.
28 P. S. Nair and G. D. Scholes, *J. Mater. Chem.*, 2006, **16**, 467–473.
29 T. Mondal, G. Piburn, V. Stavila, I. Rusakova, T. O. Ely, A. C. Colson and K. H. Whitmire, *Chem. Mater.*, 2011, **23**, 4158–4163.
30 S. L. Cumberland, K. M. Hanif, A. Javuer, G. A. Khitrov, G. F. Strouse, S. M. Woessner and C. S. Yun, *Chem. Mater.*, 2002, **14**, 1576–1584.
31 M. A. Ali, A. H. Mirza, M. H. S. A. Hamid, P. V. Bernhardt, O. Atchade, X. Song, G. Eng and L. May, *Polyhedron*, 2008, **27**, 977–984.
32 P. S. Nair, T. Radhakrishnan, N. Revaprasadu, G. A. Kolawole and P. O'Brien, *Chem. Commun.*, 2002, 564–565.
33 P. Bera, C. H. Kim and S. I. Seok, *Solid State Sci.*, 2010, **12**, 532–535.
34 P. Bera, C. H. Kim and S. I. Seok, *Solid State Sci.*, 2010, **12**, 1741–1747.
35 P. Bera and S. I. Seok, *J. Nanopart. Res.*, 2011, **13**, 1889–1896.
36 P. Bera and S. I. Seok, *Solid State Sci.*, 2012, **14**, 1126–1132.
37 G. Mondal, A. Santra, S. I. Seok and P. Bera, *J. Nanosci. Lett.*, 2014, **4**, 35.
38 G. Mondal, P. Bera, A. Santra, S. Jana, T. N. Mandal, A. Mondal, S. I. Seok and P. Bera, *New J. Chem.*, 2014, **38**, 4774–4782.
39 J. Perez and L. Liera, *Eur. J. Inorg. Chem.*, 2009, 4913–4925.
40 P. Bera, C. H. Kim and S. I. Seok, *Polyhedron*, 2008, **27**, 3433–3438.
41 M. Stoev and A. Katerski, *J. Mater. Chem.*, 1996, **6**, 377–380.
42 A. E. Saunders, A. Ghazelbash, P. Sood and B. A. Korgel, *Langmuir*, 2008, **24**, 9043–9049.
43 S. F. Wuiester, C. M. Donega and A. Meijerink, *J. Phys. Chem. B*, 2004, **108**, 17393.

